J. Chem. Sci. Vol. 126, No. 6, November 2014, pp. 1743–1751.

Sequential bond energies and structures of the $Cr^+\cdot(N_2)_n$, n =1–4

JAMAL N DAWOUD*

Department of Chemistry, Faculty of Science, Hashemite University, Zarqa 13115, P.O. Box 150459, Jordan.
e-mail: jamaldawoud@hu.edu.jo

MS received 3 February 2014; revised 29 April 2014; accepted 04 June 2014

Abstract. DFT calculations, with an effective core potential for the chromium ion and large polarized basis set functions have been used to calculate the sequential bond dissociation energies of the $Cr^+\cdot(N_2)_n$ (n = 1—4) complexes. A linear configuration was obtained for the $Cr^+\cdot N_2$ and $Cr^+\cdot(N_2)_2$ complexes with sequential bond dissociation energies of 14.6 and 16.4 kcal mol^{-1}, respectively. For the $Cr^+\cdot(N_2)_3$ and $Cr^+\cdot(N_2)_4$ complexes, distorted trigonal pyramidal and tetrahedral geometries were optimized with sequential bond dissociation energies of 6.5 and 5.5 kcal mol^{-1}, respectively. π- back-donation in side-on approach of the $Cr^+\cdot N_2$ leads to the formation of a tilted structure with the Cr^+ ion in central position. The di-ligated complex exhibits the strongest bond dissociation energy among these four $Cr^+\cdot(N_2)_n$ (n = 1—4) complexes since it has the largest Cr^+—N bond order.

Keywords. Density functional theory; nitrogen; chromium ion; bond dissociation energy; π back donation.

1. Introduction

Transition metal complexes of N_2, O_2 and CO species play an important role in organometallic syntheses, separation technology and industrial chemistry.[1–6] Further, the study of catalytic conversion of harmful gases using atomic transition metals has been receiving great attention since these gases are part of air pollution.[7,8] Bare chromium ion in different oxidation states has drawn great attention because of its importance in preventing corrosion in iron based alloys.[9] Therefore, study of chromium complexes of N_2 is of considerable interest to understand the bonding mode of these complexes and their physical and chemical properties.[10–12]

To my knowledge, the interaction of N_2 with Cr^+ ion in gas phase was not studied in details, both experimentally as well as theoretically. The $[Cr\cdot N_2]^+$ complex was prepared experimentally using laser vaporization of a solid chromium within a pulse of carrier gas including N_2 molecules.[13] The binding energy of the $Cr^+\cdot N_2$ was measured using photo-ionization spectroscopic technique and found to be 14.1 ± 0.9 kcal mol^{-1}.[13] Only one theoretical study was performed for this complex using a self-consistent field (SCF) based modified coupled-pair functional (MCPF) method.[14] The geometrical parameters and binding energy for the end-on linear structure of $Cr^+\cdot N_2$ were determined. The authors concluded that the interaction between N_2 and Cr^+ ion in gas phase is of physical nature with a binding energy of 12.2 kcal mol^{-1}.[14] Despite these efforts, there are still a number of unsettled questions including fundamental query about the nature of bonding between them. In addition, none of these theoretical and experimental studies consider the binding of more than one N_2 ligand to Cr^+ ion.

In the present work, I have undertaken a density functional theory (**DFT**) study of the $Cr^+\cdot(N_2)_n$ complexes, n = 1—4, where molecular geometries, binding energies and thermodynamic quantities are determined for end-on metal-ligand approach. The sequential bond dissociation of $Cr^+\cdot(N_2)_n$ (n = 1—4) complexes were computed and discussed in terms of the strength of electrostatic interactions within these complexes. Our results are then compared with the available experimental and theoretical data that are reported in the literature.

2. Computational Details

All the calculations were carried out using the Gaussian 03 program.[15] Geometry optimizations were calculated using a variety of DFT methods including UB3LYP, UB3P86 and UB3PW91. Pseudo potentials of "LANL2DZ and LANL2TZ" basis set function types were employed only for Cr, whereas standard all-electron Pople type 6-31+G(d) and 6-311+G(df) basis sets were utilized for the atoms of N_2 molecule. These basis sets have polarization and diffuse functions that are suitable and flexible to study the structures, binding

*For correspondence

and sequential bond dissociation energies of $Cr^+\cdot(N_2)_n$ complexes.

The intrinsic reaction coordinate (**IRC**)[16,17] and the vibration frequency tests were performed together to verify that each complex is a real minimum and then calculate the zero point energy (**ZPE**) for each stationary point and its thermodynamic properties at T = 298 K. For density functional theory (**DFT**), the binding energy was calculated by simply subtracting the total energy of the complex from the un-complexed moieties, and then corrected for basis set superposition error (**BSSE**) using the full counterpoise method.[18,19] In particular, the thermodynamic quantities, ΔH° and ΔG°, for the complex denoted as $Cr^+\cdot(N_2)_n$ may be calculated as,

$$Cr^+ + n\,N_2 \rightarrow Cr^+ \cdot (N_2)_n \qquad (n: 1—4)$$

The binding enthalpy of the $Cr^+\cdot(N_2)_n$ complex was calculated using the following formula,[20]

$$\Delta H^\circ = \sum_{products} (E_o + H)_{corr} - \sum_{reactants} (E_o + H)_{corr} \qquad (1)$$

where, $(E_o + H)_{corr}$ is the corrected electronic energy included in the zero point energy plus thermal correction to enthalpy. This term is calculated directly from the frequency test of each stationary point. The same procedure has been applied for calculating ΔG° for the $Cr^+\cdot(N_2)_n$ complex.

To have a deep insight into the electronic structure and bonding properties of the investigated complexes, the electronic parameters and Cr^+—N bond order (*BO*) of these complexes were carried out according to the natural bond orbital (NBO) analysis.[21] The amount of electronic transfer occurred within the complex was determined by taking the difference between the electronic population of the orbitals ($3d$, $4s$) of free Cr^+ ion and in complex. σ-donation involves an increase in the electronic population of the Cr^+ ion whereas the opposite trend would be attributed to the π-back donation as applied elsewhere.[12] These calculations were performed on the basis of the UB3LYP/6-311+G(df)/LANL2TZ method.

Note here, the sequential bond dissociation energies of the $Cr^+\cdot(N_2)_n$ complex are calculated according to the following equation,

$$Cr^+\cdot(N_2)_n \rightarrow Cr^+\cdot(N_2)_{n-1} + N_2 \quad (n: 1—4)$$

To explain the trend of the bond dissociation energies, the atomic charge distributions of the $Cr^+\cdot(N_2)_n$ complex at different configurations were calculated according to the natural bond orbital (**NBO**) analysis.[21] For simplicity, the charge distribution spread over an orbital centred at a particular atom is treated as a point charge at the location of the atom as applied elsewhere.[22,23] Using these point charges, the electrostatic contribution "$E^{elec.}$" to the bond dissociation energy of the $Cr^+\cdot(N_2)_n$ complex is calculated as a pair-wise sum of point charges located on each atomic site of N_2 and Cr^+ ion using the form,

$$E^{elec.} = -\frac{1}{n}\sum_{n=1}^{4}\sum_{i=1}^{2}\frac{q_{Cr^+}\cdot(q_{N_i})_n}{4\pi\varepsilon_o\cdot r_{Cr^+-N_i}} \qquad (2)$$

where, n represents the number of N_2 molecules in the complex, q_{Cr}, q_{Ni} are the point charges located on Cr^+ and N atoms separated by r_{Cr-Ni}. ε_o is the permittivity of the vacuum.

3. Results and Discussion

3.1 *Structures and binding energies of $Cr^+\cdot N_2$ complex*

The intrinsic reaction coordinates of the $Cr^+\cdot N_2$ complex ($^6\Sigma^+$ state) obtained at the UB3LYP level of theory indicate the existence of two minima and two transition states. The global minimum has a linear structure whereas the local minimum has a tilted structure. The two transition states, TS1 and TS2, exhibit L-shaped and linear structures, respectively (figure 1). Note here that side-on Cr^+—N_2 approach leads to breakdown the N≡N bond, and isomerization to the chromyl [N—Cr—N]$^+$ takes place (figure 1). The calculations of the geometry optimization results for the linear and tilted structures of the $Cr^+\cdot N_2$ complex were listed in table 1. At all levels of **DFT**, the results of the calculated geometrical parameters are in good agreement. For example, the UB3LYP/LANL2TZ/6-311+G(df) results of the geometrical parameters of the linear structure are found to be $r_{(Cr-N)}$ = 2.135 Å and $r_{(N-N)}$ = 1.094 Å, which agreed well with the MCPF optimized values[14] of the bond lengths and angles as shown in table 1.

3.2 *Electronic and bonding properties in the $Cr^+\cdot N_2$ complex*

The atomic electronic population of the corresponding orbitals in the $Cr^+\cdot N_2$ complex, in different structures were calculated and compared with those of Cr^+ ion and N_2 molecule individually before complexation. These results are summarized in table 2. For linear structure, ***Minim. 1***, the electron density of the $3d$ orbital of the Cr^+ ion was reorganized, where an electronic

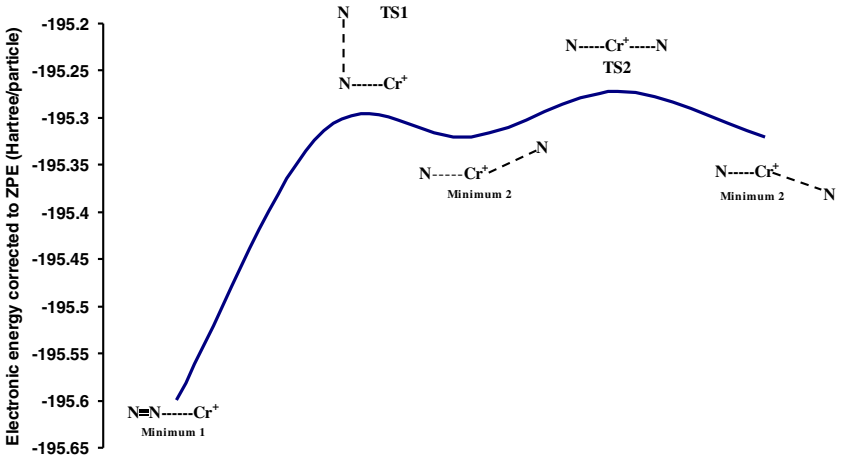

Figure 1. The IRC diagram of the $Cr^+\cdot N_2$ complex generated at the UB3LYP/LANL2TZ/6-311+G(df) level of method.

charge transfers from 3*d* orbitals [$3d^{5.00} \rightarrow 3d^{4.87}$ (linear)] toward the 4*s* orbital that its population increases by 0.133. Furthermore, a similar behaviour is observed for the N_2 moiety in the complex, where the electron density of the valence shell is slightly redistributed. It appears that the π electrons are mainly migrated toward

Table 1. Geometrical parameters[a] of linear and tilted structures of the $Cr^+\cdot N_2$ complex.

Geometry	Method	Basis set	r(N-N)	r(Cr-N)	θ(°)[b]	θ(°)[c]
Linear $Cr^+\cdot N_2$	UB3LYP	LANL2DZ/6-31+G(d)	1.105	2.138	180.0	-
		LANL2DZ/6-311+G(df)	1.094	2.155	180.0	–
		LANL2TZ/6-31+G(d)	1.107	2.139	180.0	–
		LANL2TZ/6-311+G(df)	1.094	2.135	180.0	–
Free N_2		6-311+G(df)	1.093	–	–	–
	UB3PW91	LANL2DZ/6-31+G(d)	1.105	2.168	180.0	–
		LANL2DZ/6-311+G(df)	1.094	2.151	180.0	–
		LANL2TZ/6-31+G(d)	1.105	2.138	180.0	–
		LANL2TZ/6-311+G(df)	1.094	2.132	180.0	–
Free N_2		6-311+G(df)	1.093	–	–	–
	UB3P86	LANL2DZ/6-31+G(d)	1.105	2.138	180.0	–
		LANL2DZ/6-311+G(df)	1.094	2.124	180.0	–
		LANL2TZ/6-31+G(d)	1.105	2.111	180.0	–
		LANL2TZ/6-311+G(df)	1.094	2.106	180.0	–
Free N_2		6-311+G(df)	1.092	–	–	–
Linear $Cr^+\cdot N_2$	MCPF[d]	ANO	1.096	2.249	180.0	–
	SCF[d]	ANO	1.066	2.460	180.0	–
			r(Cr-N_1)	r(Cr-N_2)		
Tilted N_1–Cr^+–N_2	UB3LYP	LANL2DZ/6-31+G(d)	2.529	1.524	–	150.8
		LANL2DZ/6-311+G(df)	2.523	1.520	–	150.7
		LANL2TZ/6-31+G(d)	2.527	1.525	–	150.8
		LANL2TZ/6-311+G(df)	2.491	1.521	–	150.5
	UB3PW91	LANL2DZ/6-31+G(d)	2.555	1.527	–	150.2
		LANL2DZ/6-311+G(df)	2.550	1.522	–	148.0
		LANL2TZ/6-31+G(d)	2.522	1.525	–	148.2
		LANL2TZ/6-311+G(df)	2.507	1.523	–	147.7
	UB3P86	LANL2DZ/6-31+G(d)	2.501	1.512	–	147.8
		LANL2DZ/6-311+G(df)	2.495	1.507	–	147.7
		LANL2TZ/6-31+G(d)	2.488	1.509	–	147.7
		LANL2TZ/6-311+G(df)	2.461	1.508	–	147.7

[a] All the bond lengths are in (Å), and the bond angles are in degrees.
[b] ∠ Cr-N1-N2 bond angle. [c] ∠ N_1-Cr-N_2 bond angle.
[d] Taken from ref. 14.

Table 2. **NBO** analysis of natural charges and 3*d*, 4*s* populations of Cr^+ ion and total population of the valence shell of each atomic site in N_2 molecule at different structures on the basis of the UB3LYP/LANL2TZ/6-311+G(df) method.

	Cr^+	N_2	$Cr^+ \cdot N_2$ (Linear, minm1)	N–Cr^+–N (tilted, minm2)
q_{Cu}	+1.000	—	+0.997	+1.130
3*d*	5.000	—	4.870	4.814
4*s*	0.000	—	0.133	0.075 {0.023, 3*d* of Cr^+ plus 0.052, 2*p* of N}
σ −donation	—	—	0.003	0.052
π −back donation	—	—	—-	0.163
$(2s, 2p_{x,y,z})$ N_1 (N_2 molecule)	—	4.952	5.158 (▲0.206)	5.163 (▲0.165)*
$(2s, 2p_{x,y,z})$ N_2 (N_2 molecule)	—	4.952	4.747 (▼0.205)	4.946 (▼0.052)*

▲: amount of increase relative to the atomic site in free N_2, ▼: amount of decrease relative to the atomic site in free N_2. * For free N atom, the electronic population of the valence orbitals $(2s, 2p_{x,y,z})$ is 4.998.

the nitrogen atom that is bounded directly with the Cr^+ ion. The population of the 3*d* orbital in the linear structure is less than 5.00 indicating a sizable electron transfer mainly to the 4*s* orbital. Such electron delocalization process indicates that 3*d*-4*s* orbitals are hybridized. The electronic population and NBO charge distributions showed that there is no electronic charge transfer between the Cr^+ and N_2 moieties and hence the interaction is of physical nature. This type of interaction may have charge-quadrupole and charge-induced dipole interactions. This was also confirmed by a small Cr^+—N bond order of 0.266 (figure 2). For tilted structure, ***Minim. 2***, a strong interaction occurred between Cr^+ ion and N_2 moieties upon complexation. The NBO analysis showed that an electronic charge transfers from 3*d* orbitals toward the 4*s* orbital, its population thus increasing by 0.023, and an electronic charge of 0.163 transfers directly to the valence orbitals of N atom indicating a strong π-back donations occurs (table 2). This was reflected by a large Cr^+—N bond order of 2.08 as shown in figure 2. This is also supported by the Cr^+–N vibration frequency of ∼890 cm^{-1} and bond length of 1.52 Å (table 1). For the second N atom, a weak σ-donation involves an electronic charge transfers from $2p_x$ and $2p_y$ of N atom towards the 4*s* orbital of Cr^+ ion and hence exhibits a small bond order of 0.068 as presented in table 2 and figure 2. As a conclusion, the electronic charge transfer in the tilted structure has a crucial effect on the bonding mode between Cr^+ ion and free N atom.

3.3 *Binding energies of the $Cr^+ \cdot N_2$ complex*

The binding energies of the $Cr^+ \cdot N_2$ in its linear structure were calculated at various levels of **DFT** methods, with the results being shown in table 3. In all cases, the results obtained by these methods are relatively consistent and reliable. My found that the linear structure exhibits a binding energy of 14.6 kcal mol^{-1} that calculated on the basis of the UB3PW91/LANL2TZ/6-311+G(df) method. My best value agreed well with 12.2 kcal mol^{-1} that was calculated by the MCPF method[14] and the experimental value[13] of 14.9 ± 0.9 kcal mol^{-1} (table 3). As expected, the local minimum $[N\text{-}Cr\text{-}N]^+$ exhibits lower binding energy than that of the global minimum Cr^+—N_2 by ∼9.5 kcal mol^{-1} as shown in table 3, which is consistent with IRC diagram presented in figure 1.

3.4 *Structures and binding energies of $Cr^+ \cdot (N_2)_n$ (n =2—4) complexes*

In this study, only end-on metal ligand complexes were examined. Thus the geometries of the end-on of the $Cr^+ \cdot (N_2)_n$ (n = 2—4) complexes were optimized at

Figure 2. **NBO** analysis of atomic charge distributions and bond order of the Cr^+—N (italic number) of the minima structures of the $Cr^+ \cdot N_2$ complex obtained on the basis of the UB3LYP/LANL2TZ/6-311+G(df) method.

Table 3. Binding energy (BE), thermodynamic quantities, ΔH°_{298} and ΔG°_{298} and BSSE, for the linear and tilted structures of $Cr^+\cdot N_2$ complex, at various levels of DFT methods. The energy units are in kcal mol^{-1}.

Geometry	Method	Basis set	BE	ΔH°_{298}	ΔG°_{298}	BSSE
Linear $Cr^+\cdot N_2$	UB3LYP	LANL2TZ/6-311+G(df)	15.8	−16.2	−9.6	1.10
	UB3PW91	LANL2TZ/6-311+G(df)	14.6	−15.1	−8.6	1.05
	UB3P86	LANL2TZ/6-311+G(df)	16.5	−17.1	−10.4	1.11
	MCPF[a]	ANO	12.2	–	–	–
	SCF[a]	ANO	7.3	–	–	–
	Exp.[b]	–	14.0 ± 0.9	–	–	–
Tilted[c] $[N\cdot Cr\cdot N]^+$	UB3LYP	LANL2TZ/6-311+G(df)	6.1	−6.4	−0.8	0.55
	UB3PW91	LANL2TZ/6-311+G(df)	5.8	−6.1	−0.4	0.58
	UB3P86	LANL2TZ/6-311+G(df)	6.5	−6.8	−1.2	0.63

[a]Taken from ref. 14. [b]Taken from ref. 13. [c] Note here the binding energy and thermodynamics data for the tilted structure were calculated according to the equation: $[N\cdot Cr\cdot N]^+ \rightarrow [Cr—N]^+ + N$.

various levels of **DFT** method and the results are shown in figure 3. A linear structure was obtained for the di-ligated complex, whereas distorted trigonal pyramidal and tetrahedral structures were found for the tri- and tetra-ligated complexes, respectively. The geometrical parameters of these complexes are presented in figure 3. It is interesting to note that the variation in the N-N bond length in these three complexes as well as the linear $Cr^+\cdot N_2$ structure was insignificant (< 0.001 Å). This is also reflected by the calculated vibration frequencies of N_2 moiety in these complexes, which showed that the four complexes exhibit the same $\omega_{(N\equiv N)}$ value of ∼2414.0 cm^{-1} [on the basis of the UB3LYP/LANL2TZ/6-311+G(df) method]. Consequently the interaction between the Cr^+ ion and N_2 moiety in an end-on approach is of physical nature.

It is worthwhile to mention here that the charge distribution of N_2 molecule plays a crucial effect on the interaction with the Cr^+ ion, since N_2 molecule has a negative quadrupole moment.[24] Thus, the negative charge was distributed on the atomic sites of N_2 molecule, whereas the positive charge was located within the bond between N atoms. Therefore, it was expected that the interaction between Cr^+ ion and N_2 moiety in a linear substructure in these complexes would be highly attractive. The natural bond orbital (**NBO**) analysis of the atomic charge distribution of the four complexes showed that the π electrons of N_2 moiety is highly polarized since the nearest nitrogen atom to Cr^+ exhibits a negative charge whereas the other one exhibits a positive charge (figure 4). Note here that Cr^+ ion still retains most of its positive charge in these four structures and hence there was no electronic transfer like σ- or π-back donations in these ion complexes. This indicates that the chromium ionic charge causes an electric field on molecular N_2 suggesting that pure electrostatic interactions may be dominant, mainly, charge-quadrupole and charge-induced dipole interactions.

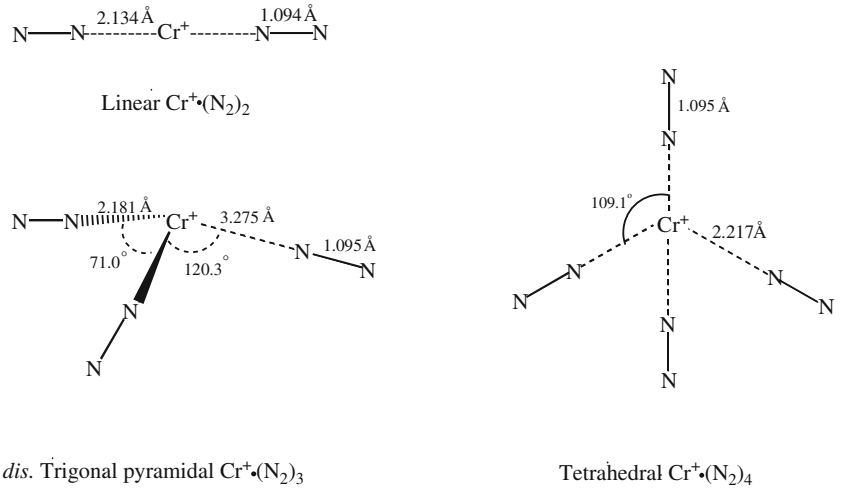

Figure 3. Optimized geometries for the minima states of the $Cr^+\cdot(N_2)_{2-4}$ complexes that obtained on the basis of the UB3LYP/LANL2TZ/6-311+G(df) method.

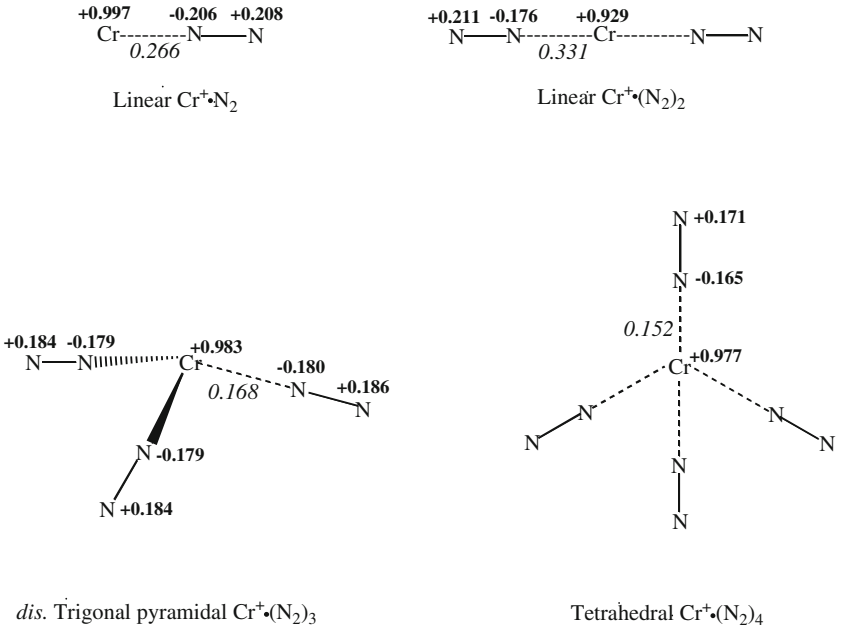

Figure 4. NBO analysis of atomic charge distributions and bond order of the Cr^+—N (italic number) of the minima structures of the $Cr^+\cdot(N_2)_{1-4}$ complexes obtained on the basis of the UB3LYP/LANL2TZ/6-311+G(df) method.

For the di-, tri- and tetra-ligated complexes, the binding energies values calculated using the UB3LYP and UB3P86 methods were consistent and in good agreement whereas the UB3PW91 calculations yielded the lowest binding energy values among these methods by ~3.0 kcal mol^{-1}. In addition, the binding energy for the minima structures increases with the number of atomic nitrogen sites that interacted directly with Cr^+ ion. As shown in table 4, the tetrahedral structure of $Cr^+\cdot(N_2)_4$, in which the Cr^+ ion is surrounded by four nitrogen atoms, has the largest binding energy among these complexes. In spite of the distorted trigonal pyramidal geometry of the $Cr^+\cdot(N_2)_3$, the separation between the Cr^+ ion and nitrogen atomic site in these three ion complexes was increased as going from di-ligated complex to tetra-ligated complex by a value of ~0.08 Å. This affected the strength of metal-ligand interaction as presented in the next section. My DFT calculations of the ΔH°_{298K} and ΔG°_{298K} values for these complexes indicated that the formation of these complexes, in their minima states, were of an exothermic process.

3.5 *Sequential bond dissociation energies of $Cr^+\cdot(N_2)_n$ (n = 1—4) complexes*

The **BDE** of $Cr^+\cdot(N_2)_n$ (n: 1—4) complexes were calculated using various DFT methods and the results were listed in table 5. In all cases, the UB3LYP and UB3PW91 computed values of the **BDE** were consistent for these chromium ion complexes, whereas the **BDE** values calculated on the basis of

Table 4. Binding energy (BE), thermodynamic quantities, ΔH° and ΔG° and BSSE, at T = 298 K for end-on approach of $Cr^+\cdot(N_2)_n$ (n = 2-4) complexes, at various levels of DFT methods. The energy units are in kcal mol^{-1}.

Geometry	Method	Basis set	BE	ΔH°	ΔG°	BSSE
Cr^+—$(N_2)_2$	UB3LYP	LANL2TZ/6-311+G(df)	33.3	−34.1	−17.6	2.32
	UB3PW91	LANL2TZ/6-311+G(df)	30.8	−31.7	−15.1	2.32
	UB3P86	LANL2TZ/6-311+G(df)	34.7	−35.7	−19.0	2.39
Cr^+—$(N_2)_3$	UB3LYP	LANL2TZ/6-311+G(df)	40.5	−41.2	−20.1	3.43
	UB3PW91	LANL2TZ/6-311+G(df)	37.3	−38.0	−16.8	3.54
	UB3P86	LANL2TZ/6-311+G(df)	42.9	−43.8	−22.3	3.67
Cr^+—$(N_2)_4$	UB3LYP	LANL2TZ/6-311+G(df)	47.1	−47.3	−19.1	4.48
	UB3PW91	LANL2TZ/6-311+G(df)	44.7	−45.3	−17.2	4.67
	UB3P86	LANL2TZ/6-311+G(df)	49.2	−49.9	−21.0	5.11

Table 5. Sequential bond dissociation energy (BDE), for the $Cr^+\cdot(N_2)_n$ complex (n: 1—4), calculated at various levels of DFT. The energy units are in kcal mol^{-1}.

Structure	Method	Basis set	BDE
The $Cr^+\cdot N_2$complex			
Linear $Cr^+\cdot N_2$	UB3LYP	LANL2TZ/6-311+G(df)	15.8
	UB3PW91	LANL2TZ/6-311+G(df)	14.6
	UB3P86	LANL2TZ/6-311+G(df)	16.5
	MCPF[a]	ANO	12.2
	Exp.[b]	–	14.0 ± 0.9
The $Cr^+\cdot(N_2)_2$complex			
$(N_2)\cdot Cr^+$— N_2 (A)	UB3LYP	LANL2TZ/6-311+G(df)	17.6
	UB3PW91	LANL2TZ/6-311+G(df)	16.4
	UB3P86	LANL2TZ/6-311+G(df)	18.3
The $Cr^+\cdot(N_2)_3$complex			
$(N_2)_2\cdot Cr^+$—N_2	UB3LYP	LANL2TZ/6-311+G(df)	7.1
	UB3PW91	LANL2TZ/6-311+G(df)	6.5
	UB3P86	LANL2TZ/6-311+G(df)	8.1
The $Cr^+\cdot(N_2)_4$complex			
$(N_2)_3\cdot Cr^+$—N_2	UB3LYP	LANL2TZ/6-311+G(df)	6.6
	UB3PW91	LANL2TZ/6-311+G(df)	5.5
	UB3P86	LANL2TZ/6-311+G(df)	7.2

[a] Taken from ref.[14]. [b] Taken from ref.[13].

the UB3P86 method were the largest among these three methods by ∼1.0 kcal mol^{-1}. Our calculations showed that the **BDE**s follow the ordering, $Cr^+\cdot(N_2)$ $<Cr^+\cdot(N_2)_2$ $>Cr^+\cdot(N_2)_3$ $>Cr^+\cdot(N_2)_4$. This was consistent with the Cr^+-N distances trend where the di-ligated complex exhibits relatively the shortest Cr^+-N distance and hence it has the strongest Cr^+—N_2 interaction. To explain the computed bond dissociation energy trend, the **NBO** analysis of the atomic charge distribution of $Cr^+\cdot(N_2)_{1-4}$ for these configurations and Cr^+—N bond order (***BO***) were calculated on the basis of the UB3LYP/LANL2TZ/6-311+G(df) method as presented in figure 4. The geometrical parameters with their atomic charges were

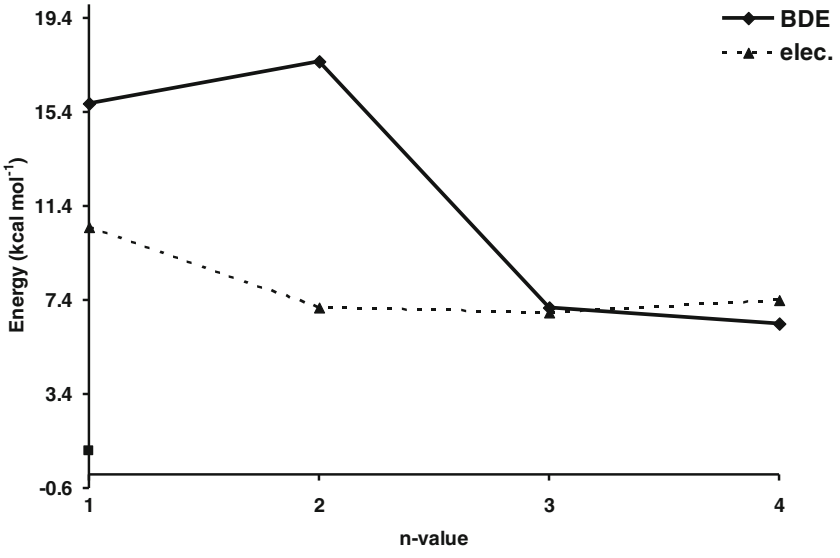

Figure 5. Bond dissociation energies (**BDE**) and their components of electrostatic, electronic energies of the $Cr^+\cdot(N_2)_n$, n = 1-4, complexes calculated on the basis of the UB3LYP/LANL2TZ/6-311+G(df) method.

used to estimate the electrostatic contribution to the bond dissociation energy using equation (2). It was noticed that the values of the ionic and atomic charges for mono-, tri- and tetra-ligated complexes were relatively the same. Consequently the small differences in the electrostatic values of these three complexes are attributed to ion-molecule separations (figure 3). The di-ligated complex exhibits the lowest ionic charge and shortest ion-molecule separation that affects oppositely the electrostatic energy values. Thus, in this model, electrostatic interactions were not changed largely and hence their contribution to the bond dissociation energy in these weakly bound complexes are not crucial to explain the computing trend as presented in figure 5. Furthermore, the repulsion among N_2 ligands in the tri- and tetra-ligated complexes ($Cr^+\cdot(N_2)_3$, $Cr^+\cdot(N_2)_4$) will push the N_2 molecule further away from the Cr^+ ion and hence reduce the bond dissociation energies in those complexes. However, the Cr^+—N bond order (***BO***) values were found to follow the same trend as that obtained for the **BDEs**, in which the di-ligated complex has relatively the largest ***BO*** value of 0.331, whereas the tetra-ligated complex exhibits the least ***BO*** value of 0.152 for the Cr^+—N as presented in figure 4. In addition, the ***BO*** values for the Cr^+—N in these four complexes are relatively small, which are consistent with the low **BDEs** values.

4. Conclusions

Density functional theory study of the end-on approach of $Cr^+\cdot(N_2)_n$ complexes, n=1—4, has been performed. Optimized structures are presented and found to agree with those from previous studies, where available. The $Cr^+\cdot N_2$ and $Cu^+\cdot(N_2)_2$ complexes exhibit linear structures, whereas distorted trigonal pyramidal and tetrahedral structures were obtained for $Cr^+\cdot(N_2)_3$ and $Cr^+\cdot(N_2)_4$, respectively. For side-on approach of the metal-ligand complex, resulted in the tilted structure, π-back donation from d^5-orbital of Cr^+ ion to $2p^3$-orbital of N atom highly affects the bonding process.

Our calculations predict that the Cr^+ ion prefers to bind in a two-fold coordination sites and hence the di-ligated complex has the highest sequential bond dissociation energy compared to the others. The **DFT** calculations showed that the variation in the electrostatic contribution to the bond dissociation energy for these complexes was insignificant. The atomic charges and Cr^+—N distances did not change largely upon going from mono- to tetra ligated complex. This result is in disagreement with the interaction between transition metal ions and polar molecules such $Cu^+\cdot(NO)_n$ complexes.[12]

Acknowledgements

JND gratefully acknowledges the financial support of the Deanship of the Scientific Research of the Hashemite University-Jordan.

References

1. Hoffmann R 1982 *Angew. Chem. Int. Ed. Engl.* **21** 711
2. Barnes L A, Rosi M and Bauschlicher, Jr. C W 1990 *J. Chem. Phys.* **93** 609
3. Cokoja M, Bruckmeier C, Rieger B, Herrmann W A and Kühn F E 2011 *Angew. Chem., Int. Ed. Engl.* **50** 8510
4. Finn C, Schnittger S, Yellowlees L J and Love J B 2012 *Chem. Commun.* **48** 1392
5. Plane J M C 2003 *Chem. Rev.* **103** 4963
6. Holland P L 2010 *Dalton Trans.* **39** 5415
7. Taylor K C 1993 *Catal. Rev. Sci. Eng.* **35** 457
8. Blagojevic V, Jarvis M J Y, Flaim E, Koyanagi G K, Lavrov V V and Bohme D K 2003 *Angew. Chem.* **115** 5073
9. Fehlner F P and Graham M J 1995 In *Corrosion Mechanisms in Theory and Practice,* P Marcus and J Odar (eds.) (New York: Marcel Dekker) p 136
10. Schultz R H, Crellin K C and Armentrout P B 1991 *J. Am. Chem. Soc.* **113** 8590
11. Griffin J B and Armentrout P B 1998 *J. Chem. Phys.* **108** 8075
12. Dawoud J N and Hassouneh T S 2014 *Monatsh. für Chem.* **145** 241
13. Lessen D E, Asher R L and Brucat P J 1991 *Chem. Phys. Lett.* **177** 380
14. Bauschlicher Jr. C W, Partridge H and Langhoff S R 1992 *J. Phys. Chem.* **96** 2475
15. Frisch M, Trucks G, Schlegel H, Scuseria G, Robb M, Cheeseman J, Montgomery J, Vreven T, Kudin K, Burant J, Millam J, Iyengar S, Tomasi J, Barone V, Mennucci B, Cossi M, Scalmani G, Rega N, Petersson G, Nakatsuji H, Hada M, Ehara M, Toyota K, Fukuda R, Hasegawa J, Ishida M, Nakajima T, Honda Y, Kitao O, Nakai H, Klene M, Li X, Knox J, Hratchian H, Cross J, Adamo C, Jaramillo J, Gomperts R, Stratmann R, Yazyev O, Austin A, Cammi R, Pomelli C, Ochterski J, Ayala P, Morokuma K, Voth G, Salvador P, Dannenberg J, Zakrzewski V, Dapprich S, Daniels A, Strain M, Farkas O, Malick D, Rabuck A, Raghavachari K, Foresman J, Ortiz J, Cui Q, Baboul A, Clifford S, Cioslowski J, Stefanov B, Liu G, Liashenko A, Piskorz P, Komaromi I, Martin R, Fox D, Keith T, Al-Laham M, Peng C, Nanayakkara A, Challacombe M, Gill P, Johnson B, Chen W, Wong M, Gonzalez C and Pople J 2003 Gaussian 03, Revision B.05, Gaussian, Inc Pittsburgh PA

16. Gonzalez C and Schlegel H B 1989 *J. Chem. Phys.* **90** 2154
17. Gonzalez C and Schlegel H B 1990 *J. Phys. Chem.* **94** 5523
18. Simon S, Duran M and Dannenberg J J 1996 *J. Chem. Phys.* **105** 11024
19. Boys S F and Bernardi F 1970 *Mol. Phys.* **19** 553
20. Alomari M I and Dawoud J N 2010 *J. Mol. Struct. (Theochem)* **939** 28
21. Bonelli B, Civalleri B, Fubini B, Ugliengo P, Otero Areán C and Garrone E 2000 *J. Phys. Chem. B* **104** 10978
22. Liu D, Wyttenbach T and Bowers M T 2004 *Int. J. Mass Spectrom.* **236** 81
23. Dawoud J N, Fasfous I I and Harahesheh T K 2014 *Comput. Theoret. Chem.* **1027** 62
24. Junquera-Hernández J M, Sánchez-Marin J and Maynau D 2002 *Chem. Phys. Lett.* **359** 343